PAPER

Check for updates

Study on the extraction of lanthanides by isomeric diglycolamide extractants: an experimental and theoretical study†

Yaoyang Liu,[a] Chuang Zhao,[a] Zhibin Liu,[a] Sheng Liu,[a] Yu Zhou,[a] Caishan Jiao,[a] Meng Zhang,[a] Yang Gao, ⓘ *[a] Hui He*[ab] and Shaowen Zhang ⓘ [c]

Two isomeric diglycolamide (DGA) extractants, N,N'-dimethyl-N,N'-dioctyl diglycolamide (L^I) and N,N-dimethyl-N',N'-dioctyl diglycolamide (L^{II}), were used to perform a comparative study on the extraction performances towards several lanthanides by extraction experiments and theoretical calculations. The experimental results show that both L^I and L^{II} show a positive sequence on the extraction of lanthanides, and L^I exhibits the higher complex ability with these lanthanides than L^{II}, except for La and Ce. Slope analysis shows that 1:2 or 1:3 complexes are formed between the two ligands and the metal ions. The geometrical structures of the complexes were optimized in the gas phase by density functional theory (DFT) on the basis of complex compositions. The results of bond lengths, MBOs and topological analysis indicated that the electrostatic interaction between metal ions and two amide O atoms in the L^{II} ligand is not as homogeneous as in L^I, and this inhomogeneity is likely to be related to the poor extraction performance of L^{II}.

Introduction

Nuclear energy, as a clean energy, can effectively cope with the problems of shortage of fossil energy and carbon emission, and has been applied in more and more countries. Safe and efficient treatment and disposal of high level liquid waste (HLLW) generated from nuclear fuel is always a large challenge and trouble for the sustainable development of nuclear energy.[1,2] A strategy of partitioning and transmutation (P&T) was proposed to separate trivalent minor actinides (MA) and other long-lived fission product elements from HLLW, and then transmute them to shorter-lived elements by neutron bombardment,[3] so that the minimization of the volume and the radio- and chemo-toxicity of HLLW can be realized.

Diglycolamides (DGAs) are considered to be promising extractants in the field of separation of HLLW due to their exceptionally high affinity for trivalent actinides (An) and lanthanides (Ln) and their benignity to the environment. Asymmetric diglycolamides (ADGAs), which have two different alkyl substituents attached to the amide N atom, in contrast to symmetric DGAs with four same alkyl substituents such as N,N,N',N'-tetraoctyl diglycolamide (TODGA) and N,N,N',N'-tetra-2-ethyl-hexyl diglycolamide (TEHDGA), have gained more and more attention recently.[4-8] The structure of DGAs, especially the alkyl substituents on the amide N atom, imposes significant influence on their physiochemical performances and extraction behaviors. For example, the DGAs with short chain alkyls such as methyl possess small space hindrance, which reduces the degree of crowding around the metal-ion bonding sites,[9] and display admirable extraction capacity to Ln(III) and An(III).[10,11] The DGAs with long chain alkyls such as octyl and dodecyl are lipophilic, and can increase the lipophilicity and the degree of solvation of the complexes in non-polar and weakly polar solvents, which is critical for the suppression of the third phase.[12] The DGAs with branched chain alkyls such as 2-ethyl-hexyl and 3,7-dimethyloctyl can not only increase the lipophilicity by virtue of increased van der Waals dispersion forces,[13,14] but also exclude some interfering metal ions.[15] Due to the existence of two kinds of alkyl substituents attached on the amide N atoms, many developed ADGAs balance superior performances in terms of alleviation of the third phase formation, excellent extractability, enough solubility in aliphatic hydrocarbon diluent and high selectivity.[7,16] For example, N,N'-dimethyl-N,N'-dihexyl-diglycolamide exhibits high extraction ability and good separation performance in the meantime.[17] N,N-didodecyl-N',N'-dioctyl-diglycolamide displays high loading concentration for nitric acid and trivalent metal ions and efficient extraction of trivalent metal ions.[18]

[a]Fundamental Science on Nuclear Safety and Simulation Technology Laboratory, College of Nuclear Science and Technology, Harbin Engineering University, Harbin, 150001, Heilongjiang Province, China. E-mail: gaoyang@hrbeu.edu.cn

[b]China Institute of Atomic Energy, P. O. Box 275 (126), Beijing, 102413, China. E-mail: hehui@ciae.ac.cn

[c]School of Chemistry and Chemical Engineering, Key Laboratory of Cluster Science of Ministry of Education, Beijing Institute of Technology, Beijing, 100081, China

† Electronic supplementary information (ESI) available: Partial extraction and stripping experiment results; molecular orbital of $[SmL_3^{II}]^{3+}$, $[HoL_3^{II}]^{3+}$, $[LuL_3^{II}]^{3+}$ analysis and Mayer bond orders analysis results. See DOI: 10.1039/d1ra07020g
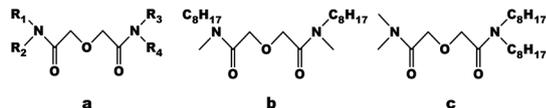
Fig. 1 (a) The structures of the asymmetric diglycolamides, (b) the structure of L^I, and (c) the structure of L^{II}.

Fig. 2 The synthetic protocol of L^{II}.

Currently, the asymmetric diglycolamides can be commonly produced in two types, and the structures are shown in Fig. 1: for one type, R1 = R3 ≠ R2 = R4; for the other type, R1 = R2 ≠ R3 = R4. The two types of diglycolamides are geometrical isomers for each other. Although extensive studies about the synthesis and extraction performances of each type of asymmetric diglycolamide have been reported, there are few studies on the differences of the two types of ADGAs. The isomers with different structures differ in electron donor ability, space steric hindrance and coordination ability, which is likely to affect their extraction performances and the structures of complexes with metal ions. Therefore, a comparative study concerning the extraction behavior and mechanism of two isomeric diglycolamides, N,N'-dimethyl-N,N'-dioctyl diglycolamide (L^I) and N,N-dimethyl-N',N'-dioctyl diglycolamide (L^{II}), whose structures are shown in Fig. 1b and c, was performed in this work by extraction experiments combined with theoretical calculations. Density functional theory (DFT) was employed to explore the geometries and chemical bonding properties of M–L (M = La, Sm, Eu, Ho, and Lu) complexes.

Experimental

Materials

Diglycolic anhydride (98%), dioctylamine (95%), dimethylamine in THF (2 M), isobutyl chloroformate (98%), 4-methylmorpholine (98%), and lanthanide nitrate hexahydrate (99.9%) were purchased from Aladdin Industrial Corporation (Shanghai, China). The other chemicals were of analytical grade and purchased from Sino pharm Reagent Co., Ltd.

The synthetic protocol of the two ligands is briefly shown in Fig. 2. The ligand L^I was synthesized by a two-step method.[19] The ligand L^{II} was prepared by the mixed acid anhydride method, and dioctyldiglycolamic acid (DODGAA) was selected as the raw material. The synthesis method has been described previously.[4]

Solvent extraction

The solvent extraction experiments about ligand L^I and various lanthanides were carried out in our previous studies;[16] therefore, the experiments concerning the extraction performance of L^{II} for lanthanide metal ions are reported here. The concentration of Ln(NO$_3$)$_3$·6H$_2$O was set at 3 mM, and the aqueous solutions were generated with a stock solution of Ln(NO$_3$)$_3$·6H$_2$O in different nitric acid concentrations. Organic phases were obtained by dissolving L^{II} in 40/60 (v/v)% n-octanol/kerosene as the diluent. The two phases were equilibrated at a 1 : 1 volume ratio with a constant-temperature shaker for
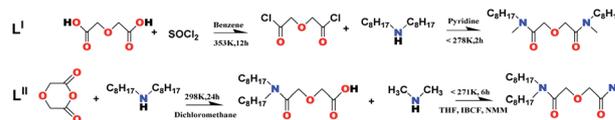
30 min. It is demonstrated that 30 min is enough for the two phases to reach equilibrium. Then the two phases were separated by centrifugation at 2500 rpm for 10 min. An aliquot of the aqueous raffinate was taken into an individual tube containing 0.1 M HNO$_3$ and the metal ion concentration was assayed by ICP-MS (X-II ICP-MS, Thermo Fisher Scientific, Waltham, MA, USA). The distribution ratio, D_{Ln}, was derived from

$$D_{Ln} = \frac{[Ln^{3+}]_{(o)}}{[Ln]_{(aq)}} \quad (1)$$

$[Ln^{3+}]_{(o)}$ and $[Ln^{3+}]_{(aq)}$ are the concentrations of Ln(III) in the aqueous phase and organic phase, respectively. The error of the data obtained in the experiment is within 5%.

Infrared spectroscopy

Infrared spectra of the L^{II} and complexes were recorded with a Spectrum 100 FT-IR (PerkinElmer, Waltham, MA, USA), and the detailed information has been described in the previous study.[9]

Theory calculations

In order to elucidate the coordination structures of metal ions with L^I and L^{II}, a series of calculations using DFT with the Gaussian 16 program package were performed.[20–22] The B3LYP was used for optimization.[23,24] The relativistic effects were considered by small-core scalar-relativistic effective core potentials (RECP), and the 28 electron core pseudopotential basis set associated with a segmented contraction scheme (ECP28MWB_SEG) was chosen for Ln(III).[25–27] For light atoms (C, H, O, and N), the polarized 6-311G(d) basis set was employed. To analyze the interaction between Ln(III) and O atoms in ligands, the topology analysis of quantum theory of atoms in molecules (QTAIM) and Mayer bond orders (MBOs) was carried out using Multiwfn software suite version 3.7.[28,29]
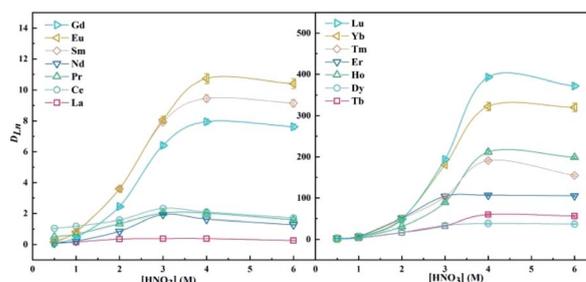

Fig. 3 Effect of HNO$_3$ on the extraction of Ln(III) by L^{II} in 40/60 (v/v)% n-octanol/kerosene (O : A = 1 : 1, $[Ln^{3+}]_{init}$ = 3 mM).

Table 1 The extraction performances of L^I and L^{II} towards Ln(III) in 3 M HNO_3

| Lanthanides	D_{Ln}	
	L^I	L^{II}
La	0.28 ± 0.01	0.38 ± 0.01
Ce	1.51 ± 0.01	2.32 ± 0.02
Pr	2.93 ± 0.02	2.01 ± 0.03
Nd	4.81 ± 0.03	3.93 ± 0.03
Sm	32.49 ± 0.03	7.91 ± 0.09
Eu	49.21 ± 0.09	8.08 ± 0.23
Gd	78.04 ± 0.23	6.41 ± 0.132
Tb	162.82 ± 1.13	32.78 ± 1.28
Dy	222.64 ± 1.27	33.59 ± 1.34
Ho	576.38 ± 3.33	89.32 ± 1.89
Er	945.35 ± 3.89	103.91 ± 1.23
Tm	975.70 ± 9.23	102.13 ± 2.02
Yb	1035.87 ± 10.88	180.50 ± 1.80
Lu	1351.16 ± 10.27	193.56 ± 2.24
Literature	16	Previous study

Results and discussion

Solvent extraction

Effect of nitric acid concentration. The initial acidity of the aqueous phase is one of the important factors affecting the distribution ratios of lanthanides. The variation trends of the distribution ratios of Ln(III) with acidity in the range of 0.5 M to 6 M HNO_3 are shown in Fig. 3, and the results show that D_{Ln} increases and then slightly decreases, and the maximum value of D_{Ln} appears at about 3.0 M or 4.0 M HNO_3. The increasing trends in the distribution ratio are caused by the salting out of NO_3^- when the acidity is not very high.[19,30,31] The competitive effect of H^+ plays an important role in inhibiting the extraction of Ln(III) when the concentration of HNO_3 is high. Third phase formation was not observed during all the extraction processes.

The distribution ratios of Ln(III) with different atomic numbers are shown in Fig. S1.† It is clear that D_{Ln} increases with the increase of the atomic number. From the point of view of spatial structure, due to the lanthanide shrinkage effect, the charge density of lanthanide ions increases as the ion radius decreases, resulting in a stronger interaction between heavy

lanthanide ions and the ligand than that between light lanthanide ions and the ligand. The comparison of the distribution ratios of lanthanides with L^I and L^{II} as the extractants at 3 M HNO_3 is listed in Table 1. The results show that the extraction performance of L^{II} for La and Ce is better than that of L^I, and the extraction performance of L^I for heavy lanthanides is much better than that of light lanthanides.

Effect of ligand concentration. As shown in Fig. 4, the distribution ratios of Ln(III) exhibit an increasing trend as the concentration of ligand L^{II} increases from 0.024 M to 0.12 M. The general extraction reaction equation of the DGA class extractant can be expressed as[6,32]

$$Ln_{(aq)}^{3+} + 3NO_{3\ (aq)}^- + nL_{(o)}^{II} \leftrightarrow Ln(NO_3)_3 \cdot nL_{(o)}^{II} \quad (2)$$
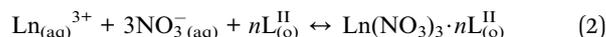
where the subscripts (aq) and (o) denote the aqueous and organic phases, respectively.

The extraction equilibrium constant K can be expressed as

$$K = \frac{\left[Ln(NO_3)_3 \cdot nL^{II}\right]_{(o)}}{\gamma_{Ln^{3+}} \gamma_{NO_3^-}^3 \left[Ln^{3+}\right]_{(aq)} \left[NO_3^-\right]_{(aq)}^3 \left[L^{II}\right]_{(o)}^n}$$

$$= \frac{\left[Ln(NO_3)_3 \cdot nL^{II}\right]_{(o)}}{\gamma_{\pm Ln(NO_3)_3}^4 \left[Ln^{3+}\right]_{(aq)} \left[NO_3^-\right]_{(aq)}^3 \left[L^{II}\right]_{(o)}^n} = \frac{D_{Ln}}{\gamma_{\pm Ln(NO_3)_3}^4 \left[NO_3^-\right]_{(aq)}^3 \left[L^{II}\right]_{(o)}^n}$$

$$(3)$$

where $[L^{II}]_{(o)}$ and $[Ln(NO_3)_3 \times nL^{II}]_{(o)}$ are the concentrations of the free extractant and the complexes in the organic phase, respectively. $[Ln^{3+}]_{(aq)}$ and $[NO_3^-]_{(aq)}$ are the concentrations of Ln(III) and NO_3^- in the aqueous phase, respectively. $\gamma_{Ln^{3+}}$ and $\gamma_{NO_3^-}$ are the ionic activity coefficients of Ln(III) and NO_3^-, respectively, and $\gamma_{\pm Ln(NO_3)_3}$ is the average ionic activity coefficient of $Ln(NO_3)_3$. $\gamma_{\pm Ln(NO3)3}$ can be addressed using a simplified Pitzer model in mixed electrolyte solutions,[33–35] and the related parameters and the average activity coefficients have been solved in previous studies.[16]

Rearranging eqn (3) in the logarithmic form will give

$$\lg D_{Ln} = n \times \lg[L^{II}]_{(o)} + \lg K \gamma_{\pm Ln(NO_3)_3}^4 [NO_3^-]_{(aq)}^3 \quad (4)$$

According to eqn (4), the number of extractant molecules in the complexes, 'n', could be obtained by the slope analysis method, as shown in Fig. 4. It can be seen that the slopes of La,
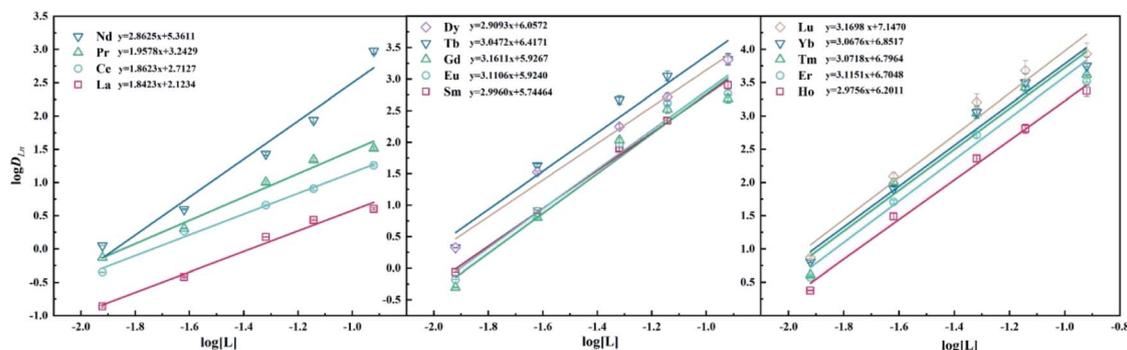
Fig. 4 Dependency of $\log D_{Ln}$ on extractant concentration in 40/60 (v/v)% n-octanol/kerosene (O : A = 1 : 1), $[Ln^{3+}]_{init}$ = 3 mM, $[L^{II}]$ = 0.012–0.12 M.

Fig. 5 Dependency of log K on extractant concentration in 40/60 (v/v)% n-octanol/kerosene (O : A = 1 : 1), $[Ln^{3+}]_{init}$ = 3 mM, $[L^{II}]$ = 0.012–0.12 M.

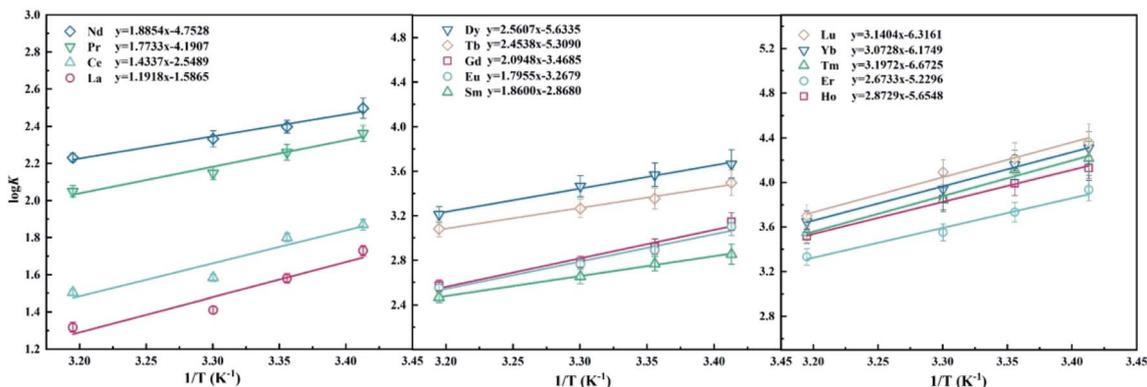Table 2 The calculated thermodynamic data of extraction reactions of Ln(III) ([L] = 0.024 M, $[HNO_3]$ = 3 M, O : A = 1 : 1)

Ln(III)	L^{II}			L^{I}
	ΔH (kJ mol^{-1})	ΔS (J mol^{-1} K^{-1-1})	ΔG (kJ mol^{-1})	ΔG (kJ mol^{-1})
La	-22.82 ± 0.31	-30.38 ± 2.21	-13.77 ± 0.50	-10.28 ± 0.22
Ce	-27.45 ± 0.34	-48.80 ± 3.29	-12.91 ± 0.41	-10.58 ± 0.34
Pr	-33.95 ± 0.67	-80.24 ± 4.78	-10.04 ± 0.38	-12.90 ± 0.41
Nd	-36.10 ± 0.87	-64.55 ± 4.92	-15.46 ± 0.34	-17.31 ± 0.55
Sm	-35.61 ± 1.27	-54.91 ± 3.27	-19.25 ± 1.01	-28.45 ± 0.67
Eu	-34.38 ± 1.01	-62.57 ± 4.66	-15.73 ± 0.44	-30.09 ± 0.62
Gd	-40.11 ± 2.11	-66.41 ± 4.56	-20.32 ± 1.54	-29.13 ± 1.05
Tb	-46.98 ± 1.88	-101.65 ± 5.20	-16.69 ± 1.45	-33.21 ± 1.87
Dy	-49.03 ± 2.13	-107.87 ± 6.00	-16.89 ± 2.00	-34.00 ± 1.82
Ho	-55.01 ± 2.71	-108.27 ± 6.87	-22.74 ± 1.99	-35.34 ± 2.00
Er	-51.19 ± 2.81	-100.13 ± 5.94	-21.35 ± 1.84	-36.26 ± 1.88
Tm	-61.22 ± 2.09	-127.76 ± 4.88	-23.14 ± 1.52	-37.04 ± 2.03
Yb	-58.84 ± 2.01	-118.23 ± 5.98	-23.60 ± 1.59	-36.62 ± 2.05
Lu	-60.13 ± 3.11	-120.94 ± 5.78	-24.09 ± 2.01	-37.18 ± 2.11
Ref.	Present work			16

Ce, and Pr are all around 2, indicating that the stoichiometric ratios of the extracted species are 1 : 2. As for other lanthanides, the slopes are around 3; it is demonstrated that 1 : 3 of M:L^{II} complexes exist in the organic phase. In the study of ligand L^{I}, 2–3 stoichiometry for different lanthanides has also been obtained.[16]

Thermodynamics of extraction. The thermodynamic parameters for the extraction of Ln(III) by L^{II} can be obtained by eqn (5) and Van't Hoff equation eqn (6):

$$\lg K = \lg \frac{D_{Ln}}{\gamma_{\pm Ln(NO_3)_3}^4 [NO_3^-]_{(aq)}^3 [L^{II}]_{(o)}^n} = -\frac{\Delta H}{2.303RT} + \frac{\Delta S}{2.303R} \tag{5}$$

$$\Delta G = \Delta H - T\Delta S \tag{6}$$

The values of ΔH and ΔS could be obtained by the values of the slope and intercept of the linear fitting equation of $1/T$ vs. log K. As shown in Fig. 5, the lower temperature corresponds to

a larger equilibrium constant of the extraction reaction, indicating that the coordination of L^{II} with lanthanides is an exothermic process, which is consistent with the previous studies.[6]

The thermodynamic data of the coordination reaction of different lanthanides with L^{I} and L^{II} are shown in Table 2. The negative values of ΔG indicate that the extraction reactions were spontaneous. As the atomic number increases, the ΔG values show a decreasing trend, suggesting that heavy lanthanides are more preferably extracted. Additionally, for the two metal ions of La and Ce, the ΔG value of L^{I} is larger than that of L^{II}, and for the ΔG values of Pr–Lu, L^{I} is less than L^{II}. Therefore, L^{I} exhibits better extraction performance for heavy lanthanides.

Striping behavior of Ln(III) by nitric acid. The stripping efficiencies of La(III), Nd(III), Eu(III), Dy(III), and Tm(III) by deionized water and various concentrations of HNO_3 are shown in Fig. S2.† The results show that, similar to the extraction system with L^{I} as the extractant, 0.001 M HNO_3 also exhibits the best stripping efficiency for the L^{II} extraction system loaded with
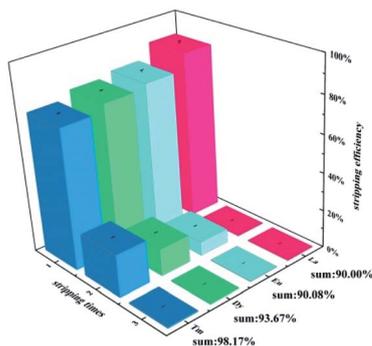
Fig. 6 Effect of the times of stripping on the stripping efficiency of La(III), Eu(III), Dy(III), and Tm(III) by nitric acid, O : A = 1 : 1, [HNO₃] = 0.001 M.
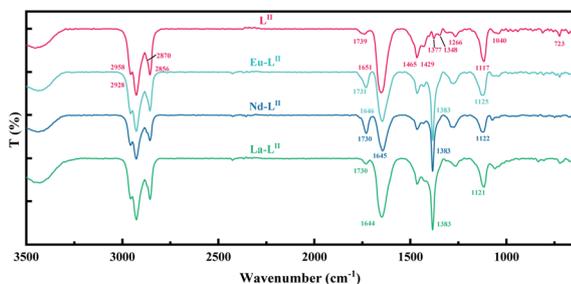

Fig. 7 The FT-IR of the ligand and the complexes.

metal ions. The stripping efficiencies of different lanthanides with 0.001 M HNO₃ are shown in Fig. S3,† and generally heavy lanthanides are more difficult to strip, which is consistent with the extraction results.

Besides, the stripping efficiencies of all lanthanides can reach more than 70% after a single stripping. This case is different from the **L**^{I} ligand, and the single stripping efficiency of **L**^{I} for heavy lanthanides can only reach 35%.[16] It implies that the interaction between **L**^{I} ligands and heavy lanthanides is stronger. The effect of the times of stripping on the stripping efficiencies of La(III), Eu(III), Dy(III), and Tm(III) is shown in Fig. 6. All stripping efficiencies can reach 90% after three times of stripping.

Infrared spectroscopy studies. The FT-IR spectra of the ligand **L**^{II} and the corresponding complexes are shown in Fig. 7. For the pure **L**^{II} ligand, the absorption peaks at 2800 cm^{-1} to 3000 cm^{-1} correspond to the –CH₃ asymmetric stretching vibration and symmetric stretching vibration. The peak at 1651 cm^{-1} is the symmetric stretching vibration of the amide carbonyl C=O, which also exists in symmetric DGAs, such as TODGA or TEHDGA, and **L**^{I} type asymmetric DGAs. Different from **L**^{I}, there is a new absorption band around the frequency of 1739 cm^{-1} (1700–1780 cm^{-1}) in the IR spectra of **L**^{II}, which seems to be also the symmetric stretching vibration of C=O. In a DGA molecule, the conjugation effect and induction effect exist in the amide group at the same time, and the strong conjugation effect of N weakens the amide C=O double bond. For the **L**^{II} ligand, the kind of the alkyl substituents connected

to the two amide groups is different, and the weakening degree of the two C=O bonds is different due to the difference in the induction effect of the two alkyl groups. Therefore, there exists a clear split in the absorption band of C=O stretching vibration. The bands with higher frequency and lower frequency correspond to the asymmetric and symmetric coupling vibrations of C=O, respectively. The low frequency band is wider and stronger than the high frequency. After coordination with lanthanides, the peaks at 1739 cm^{-1} and 1651 cm^{-1} are both blue shifted, which indicates that both bands correspond to C=O stretching vibration.

In addition, 1465 cm^{-1} and 1429 cm^{-1} are C–N stretching vibration, which belongs to amide III bands; 1377 cm^{-1} and 1348 cm^{-1} may belong to variable-angle vibrations of H–C–H; 1266 cm^{-1} belongs to amide II bands or amide III bands. The asymmetric and symmetric stretching vibrations of the ether bond coincide, so the obvious peak can be only observed at 1117 cm^{-1}; the amide V bands or amide VII bands at 723 cm^{-1} and 1040 cm^{-1} correspond to the O=C–N in-plane bending vibration or out-of-plane bending vibration.

In the infrared spectrum of the organic phase loaded with metal ions, the absorption peaks of C=O have a different degree of blue shift compared to the pure extractant, from 1739 cm^{-1}/1649 cm^{-1} of pure **L**^{II} to 1730 cm^{-1}/1644 cm^{-1} (La), 1730 cm^{-1}/1645 cm^{-1} (Nd), and 1731 cm^{-1}/1647 cm^{-1} (Eu), respectively. The symmetric stretching absorption peaks of the ether O bond shift from 1117 cm^{-1} of pure **L**^{II} to 1121 cm^{-1} (La), 1122 cm^{-1} (Nd) and 1125 cm^{-1} (Eu), respectively.[36] It indicates that the **L**^{II} molecule can form tridentate complexes with La(III), Nd(III), and Eu(III) through two carbonyl groups and one ether group. The studies by Kou *et al.* illustrated the structure of the complex between **L**^{I} and Eu(III),[16,37,38] and the results showed that Eu(III), in the center of the complex, is surrounded by three **L**^{I} molecules with tridentate coordination, and the **L**^{II} complex also has a similar structure.

Theoretical calculation

A series of scalar-relativistic density functional theory calculations were carried out to explain the difference of complexing abilities between **L**^{I} and **L**^{II}. Firstly, the properties of the ligands were analyzed according to HSAB (Hard Soft Acid Base) theory. The hardness (η) is one of the parameters to judge the complexing ability between ligands and metal ions. η can be determined by eqn (7):

$$\eta = (IP - EA)/2 \qquad (7)$$

where IP and EA represent the vertical ionization potential and vertical electron affinity of the neutral ligands, respectively. The η value of **L**^{I} and **L**^{II} is 3.805 and 3.784, respectively, indicating that the alkalinity of **L**^{I} is harder. As the atomic number of the lanthanides increases, the positive charge density increases, and the acid hardness of the lanthanide metal ions gradually increases. Therefore, the ligand **L**^{I} has better extraction performance for heavy lanthanides according to HSAB theory.

Optimized structures of the M–L complexes. The complex structures were optimized at the B3LYP/6-311G(d)/RECP level of
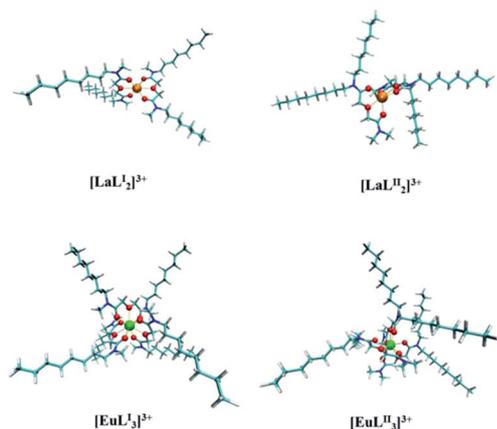
Fig. 8 The optimized complex structure of M–L^I/L^{II} (M = La, Eu); orange-La, green-Eu, cyan-carbon, white-hydrogen, red-oxygen, and blue-nitrogen.

theory using Gaussian 16. Since nitrates are in the second coordination layer, they are ignored in the optimization of the complex structures, and the dominant species are $[M \times nL]^{3+}$ (M = La–Pr, $n = 2$; M = Nd–Lu, $n = 3$). Fig. 8 shows the optimized structures of the complexes of La and Eu with L^I and L^{II}, and the structures of the other complexes such as Sm, Ho, and Lu are shown in Fig. S4.† Both L^I and L^{II} are coordinated with lanthanide ions as a tridentate ligand, which is in agreement with the previous studies.[36,39]

The bond lengths of M–O_{ether}, M–O_{amide1}, and M–O_{amide2} and the average bond lengths of all bonds are listed in Table 3. The results show that generally the M–O_{ether} bond lengths are longer than the M–O_{amide1} and M–O_{amide2} bond lengths for the same metal ion, and the bond lengths of Ln–O_{ether}, Ln–O_{amide1} and M–O_{amide2} decrease with the increase of the atomic number of lanthanides. Except that the average bond length of La–L^{II} is slightly less than that of La–L^I, the average bond lengths of other M–L^{II} (M = Sm, Eu, and Ho) complexes are slightly less

Table 3 Average M–O_{ether}, M–O_{amide1} and M–O_{amide2} bond lengths of M–L complexes (M = La, Sm, Eu, Ho, and Lu) at the B3LYP/6-311G(d)/RECP level of theory

Elements	Bond	L^I		L^{II}	
La	M–O_{ether}	2.724	2.5794	2.656	2.5159
	M–O_{amide1}	2.507		2.457	
	M–O_{amide2}	2.507		2.435	
Sm	M–O_{ether}	2.620	2.4854	2.622	2.4859
	M–O_{amide1}	2.418		2.430	
	M–O_{amide2}	2.418		2.406	
Eu	M–O_{ether}	2.600	2.4699	2.601	2.4701
	M–O_{amide1}	2.405		2.395	
	M–O_{amide2}	2.405		2.414	
Ho	M–O_{ether}	2.558	2.4230	2.561	2.4235
	M–O_{amide1}	2.356		2.343	
	M–O_{amide2}	2.355		2.366	
Lu	M–O_{ether}	2.509	2.3816	2.513	
	M–O_{amide1}	2.318		2.309	2.3823
	M–O_{amide2}	2.318		2.325	

Table 4 The electron density $\rho(r)$ and Laplacian $\nabla^2\rho(r)$ at the M–O_{ether} and M–O_{amide} (M = La, Sm, Eu, Ho, and Lu) bond critical point (BCP) at the B3LYB/6-311G(d)/RECP level of theory

Bond	L^I		L^{II}	
	Average $\rho(r)$	Average $\nabla^2\rho(r)$	Average $\rho(r)$	Average $\nabla^2\rho(r)$
La–O_{amide1}	0.0452	0.1701	0.0465	0.1769
La–O_{amide2}	0.0452	0.172	0.0438	0.1677
La–O_{ether}	0.0266	0.1083	0.0269	0.124
Sm–O_{amide1}	0.0488	0.2024	0.0474	0.1973
Sm–O_{amide2}	0.0488	0.2021	0.0503	0.2078
Sm–O_{ether}	0.0292	0.1309	0.0291	0.1303
Eu–O_{amide1}	0.0491	0.2066	0.0511	0.2142
Eu–O_{amide2}	0.0489	0.2064	0.047	0.1992
Eu–O_{ether}	0.0292	0.1327	0.0291	0.1324
Ho–O_{amide1}	0.0509	0.2256	0.0529	0.2403
Ho–O_{amide2}	0.0509	0.2256	0.0494	0.2231
Ho–O_{ether}	0.0312	0.1458	0.0304	0.1468
Lu–O_{amide1}	0.0515	0.2359	0.0528	0.2417
Lu–O_{amide2}	0.0515	0.2359	0.0504	0.2316
Lu–O_{ether}	0.0312	0.1492	0.0301	0.1477

than those of M–L^I complexes. There is an 'imbalance' in the bond length between metal ions and the amide O atoms in the L^{II} ligand, and the difference of the bond lengths between M–O_{amide1} and M–O_{amide2} in M–L^{II} is larger than in M–L^I. Moreover, the difference of the electrostatic potential of O_{amide1} and O_{amide2} in L^{II} is also larger than that in L^I.[36] So there exists a larger difference in the ability of electron-donation of the two amide O atoms in L^{II} than in L^I. The calculation results of Mayer bond orders (MBOs) of M–O_{ether}, M–O_{amide1} and M–O_{amide2} (M = La, Sm, Eu, Ho, and Lu) are listed in Table S1,† in which the 'imbalance' phenomenon of L^{II} also exists. MBOs of M–O_{amide1} and M–O_{amide2} in L^I are almost the same, but MBOs of M–O_{amide1} and M–O_{amide2} in L^{II} are different. All MBO values are within the range of 0.10–0.34, indicating that the interactions between the ligands and the metal ions display weak covalency.[40,41]

Topology analysis. The average electron density $\rho(r)$ and Laplacian $\nabla^2\rho(r)$ at the M–O_{ether}, M–O_{amide1} and M–O_{amide2} bond critical point (BCP) of five complexes are listed in Table 4. According to the QTAIM theory, $\rho(r) > 0.2$ a.u. and $\nabla^2\rho(r) < 0$ at the BCPs represent a covalent interaction, and an ionic interaction corresponds to $\rho(r) < 0.1$ a.u. and $\nabla^2\rho(r) > 0$ at the BCPs. The $\rho(r)$ values at M–O_{amide1}, M–O_{amide2} and M–O_{ether} BCPs are <0.1 a.u. and all $\nabla^2\rho(r)$ values are positive. Therefore, all of these bonds are ionic bonds. Combining electrostatic potential analysis, bond length, bond order and electron density, it is found that coordination ability of the ether oxygen bond in the two ligands is weaker than that of the two amide O atoms, and the coordination ability of the amide O atoms in the L^{II} ligand is weaker than that of L^I, which is reflected in the difference of their extraction performances.

Molecular orbital (MO) analysis. In order to further learn the bonding nature of the complexes of two ligands and Ln(III), MO analysis was carried out. The α-spin valence MO diagrams of $(ML^I)^{3+}$ and $(ML^{II})^{3+}$ (M = La, Sm, Eu, Ho, and Lu) were obtained
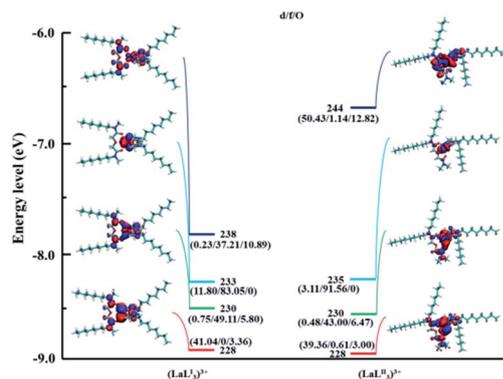
Fig. 9 The energy levels (eV) of the α-spin valence MOs and the corresponding diagrams in the $[LaL_2]^{3+}$ complexes (isosurface value: 0.02 a.u.).

to evaluate the involvement extent of various molecular orbitals for coordination. Fig. 9, 10, S5, S6, and S7† show the α-spin valence MO diagrams of the $[LaL_2]^{3+}$, $[EuL_3]^{3+}$, $[SmL_3]^{3+}$, $[HoL_3]^{3+}$, and $[LuL_3]^{3+}$, respectively, and the contribution of specific atoms to several representative molecular orbitals. d/f/O represent the 5d orbitals and 4f orbitals of lanthanides, and the 2p orbitals of O_{amide1}, O_{amide2} and O_{ether}, respectively. It can be seen that the lanthanide ions have orbital interactions with amide O atoms compared to ether O atoms, which demonstrates that the amide O atoms have the stronger complex ability. The composition of MO # 230, MO # 238 in the $(LaL_2^I)^{3+}$ complex and MO # 230, MO # 235 in the $(LaL_2^{II})^{3+}$ complex, MO # 341 in the $(EuL_3^I)^{3+}$ complex, and 341 in the $(EuL_3^{II})^{3+}$ complex is mainly composed of the 4f orbital. In Fig. 10, the 4f orbital component in the molecular orbital of the complex formed by L^{II} and La has the largest component 4f orbitals (91.56%, MO # 235, $(LaL_2^{II})^{3+}$), which is larger than the complex formed by L^I and La (83.05%, MO # 233, $(LaL_2^I)^{3+}$). However, for the Sm, Eu, Ho, and Lu the corresponding L^I complexes possess MOs with the largest component 4f orbital. Similar results can be observed in the analysis of the component of 2p orbital in O atoms. Therefore, it seems that there exist less electron sharing
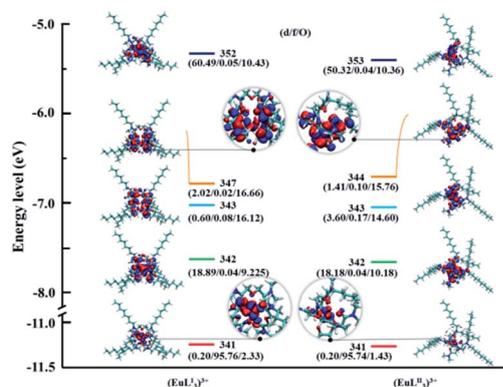

Fig. 10 The energy levels (eV) of the α-spin valence MOs and the corresponding diagrams in the $[EuL_3]^{3+}$ complexes (isosurface value: 0.02 a.u.).

and weaker interactions between heavy lanthanides and L^{II},[42] which is probably caused by different electron donating capabilities of the two amide O atoms in the L^{II} ligand.

Conclusions

A comparative study of the extraction behavior towards several lanthanides by N,N′-dimethyl-N,N′-dioctyl diglycolamide (L^I) and N,N-dimethyl-N′,N′-dioctyl diglycolamide (L^{II}) in 40/60 (v/v)% n-octanol/kerosene was carried out. Extraction thermodynamic results suggest that all extraction reactions are exothermic and both ligands exhibit positive sequential extraction of lanthanides, and L^{II} has poorer extraction performance for these lanthanides except for La and Ce than L^I. Analysis by the slope method and FT-IR analysis show that L^{II} forms 1:2 complexes (La, Ce, and Pr) and 1:3 complexes (Nd–Lu) by two amide O atoms and one ether O atom, which is similar to L^I.

To further elucidate the reason for the differences in the extraction performances of Ln(III), the DFT method was used to explore the structure of the complexes and the interaction between Ln(III) with amide and ether O atoms in L^I and L^{II}. The bond length, MBO and MO analysis demonstrate that except for La, the interaction between these lanthanides and L^{II} is weaker than that for L^I, which is in agreement with the experiment results. In particular, there exists "imbalance" in the bonding lengths and Mayer bond orders of metal ions and the two amide O atoms in L^{II}, which is responsible partially for the poor extraction performances of L^{II}. The study is expected to be helpful for evaluating the coordination ability of two types of isomeric asymmetric diglycolamides and further exploring the structure–performance relationship of diglycolamide extractants.

Author contributions

Yaoyang Liu: investigation, data curation, and writing – original draft. Chuang Zhao: investigation. Zhibin Liu: investigation. Sheng Liu: methodology. Yu Zhou: resource. Caishan Jiao: supervision and funding acquisition. Meng Zhang: supervision. Yang Gao: investigation, writing – review & editing, resources, and funding acquisition. Hui He: supervision, funding acquisition, and conceptualization. Shaowen Zhang: software.

Conflicts of interest

There are no conflicts to declare.

Acknowledgements

Notes and references

1 W. Yao, Y. Wu, H. Pang, X. Wang, S. Yu and X. Wang, *Sci. China: Chem.*, 2018, **61**, 812–823.

2 V. Manchanda, *Sep. Purif. Technol.*, 2004, **35**, 85–103.

3 M. Salvatores, *Nucl. Eng. Des.*, 2005, **235**, 805–816.

4 J. Ravi, T. Prathibha, K. A. Venkatesan, M. P. Antony, T. G. Srinivasan and P. R. Vasudeva Rao, *Sep. Purif. Technol.*, 2012, **85**, 96–100.

5 Y. Shen, X. Tan, L. Wang and W. Wu, *Sep. Purif. Technol.*, 2011, **78**, 298–302.

6 Y. Liu, Z. Liu, C. Zhao, Y. Zhou, Y. Gao and H. He, *Prog. Chem.*, 2020, **21**, 219–229.

7 J. Ravi, K. A. Venkatesan, M. P. Antony, T. G. Srinivasan and P. R. Vasudeva Rao, *Radiochim. Acta*, 2014, **102**, 609–617.

8 P. K. Mohapatra, A. Sengupta, M. Iqbal, J. Huskens and W. Verboom, *Chem.–Eur. J.*, 2013, **19**, 3230–3238.

9 Y. Liu, Y. Gao, Z. Wei, Y. Zhou, M. Zhang, H. Hou, G. Tian and H. He, *J. Radioanal. Nucl. Chem.*, 2018, **318**, 2087–2096.

10 H. Cui, X. Feng, J. Shi, W. Liu, N. Yan, G. Rao and W. Wang, *Sep. Purif. Technol.*, 2020, **234**, 116096.

11 X. Peng, Y. Li, J. Ma, Y. Cui and G. Sun, *J. Radioanal. Nucl. Chem.*, 2017, **313**, 327–332.

12 K. R. Swami, K. A. Venkatesan and M. P. Antony, *Solvent Extr. Ion Exch.*, 2019, **37**, 500–517.

13 K. R. Swami and K. A. Venkatesan, *J. Mol. Liq.*, 2019, **296**, 111741.

14 P. R. Schreiner, L. V. Chernish, P. A. Gunchenko, E. Y. Tikhonchuk, H. Hausmann, M. Serafin, S. Schlecht, J. E. Dahl, R. M. Carlson and A. A. Fokin, *Nature*, 2011, **477**, 308–311.

15 D. Stamberga, M. R. Healy, V. S. Bryantsev, C. Albisser, Y. Karslyan, B. Reinhart, A. Paulenova, M. Foster, I. Popovs, K. Lyon, B. A. Moyer and S. Jansone-Popova, *Inorg. Chem.*, 2020, **59**, 17620–17630.

16 Y. Liu, C. Zhao, Z. Liu, Y. Zhou, C. Jiao, M. Zhang, H. Hou, Y. Gao, H. He and G. Tian, *J. Radioanal. Nucl. Chem.*, 2020, **325**, 409–416.

17 Y. Sasaki and G. R. Choppin, *J. Radioanal. Nucl. Chem.*, 1996, **12**, 225–230.

18 J. Ravi, K. A. Venkatesan, M. P. Antony, T. G. Srinivasan and P. R. Vasudeva Rao, *J. Radioanal. Nucl. Chem.*, 2012, **295**, 1283–1292.

19 S. Guoxin, L. Min, C. Yu, Y. Meilong and Y. Shaohong, *Solvent Extr. Ion Exch.*, 2010, **28**, 482–494.

20 M. Frisch, G. Trucks, H. Schlegel, G. Scuseria, M. Robb, J. Cheeseman, G. Scalmani, V. Barone, G. Petersson and H. Nakatsuji, *Gaussian 16 (Revision B.01)*, Gaussian Inc.,Pittsburgh, PA, 2016.

21 R. Nityananda, P. Hohenberg and W. J. R. Kohn, *Resonance*, 2017, **22**, 809–811.

22 J. Perdew., *Phys. Rev. B: Condens. Matter Mater. Phys.*, 1986, **33**, 8822–8824.

23 B. D. Axel, *Phys. Rev. B: Condens. Matter Mater. Phys.*, 1998, **98**, 5648–5652.

24 C. Lee, W. Yang and R. G. Parr, *Phys. Rev. B: Condens. Matter Mater. Phys.*, 1988, **37**, 785.

25 M. Dolg, H. Stoll and H. J. Preuss, *J. Chem. Phys.*, 1989, **90**, 1730–1734.

26 W. Küchle, M. Dolg, H. Stoll and H. Preuss, *J. Chem. Phys.*, 1994, **100**, 7535–7542.

27 X. Cao and M. Dolg, *J. Mol. Struct.*, 2002, **581**, 139–147.

28 T. Lu and F. J. Chen, *J. Comput. Chem.*, 2012, **33**, 580–592.

29 T. Lu and S. Manzetti, *J. Struct. Chem.*, 2014, **25**, 1521–1533.

30 F. McLachlan, K. Greenough, A. Geist, B. McLuckie, G. Modolo, A. Wilden and R. Taylor, *Solvent Extr. Ion Exch.*, 2016, **34**, 334–346.

31 E. A. Mowafy and H. F. Aly, *Solvent Extr. Ion Exch.*, 2007, **25**, 205–224.

32 A. N. Turanov and V. K. Karandashev, *Solvent Extr. Ion Exch.*, 2018, **36**, 257–271.

33 K. Pitzer, *J. Phys. Chem.*, 1973, **77**, 268–277.

34 K. S. Pitzer and G. Mayorga, in *Molecular Structure And Statistical Thermodynamics: Selected Papers of Kenneth S Pitzer*, World Scientific, 1993, pp. 396–404.

35 K. S. Pitzer, *Activity Coefficients in Electrolyte Solutions*, CRC press, 2018.

36 Y. Liu, S. Liu, Z. Liu, C. Zhao, C. Li, Y. Zhou, C. Jiao, Y. Gao, H. He and S. Zhang, *RSC Adv.*, 2021, **11**, 27969–27977.

37 F. Kou, S. Yang, H. Qidan, L. Zhang, C. M. Beavers, S. J. Teat and G. Tian, *Dalton Trans.*, 2016, **45**, 18484–18493.

38 F. Kou, S. Yang, L. Zhang, S. J. Teat and G. Tian, *Inorg. Chem. Commun.*, 2016, **71**, 41–44.

39 E. A. Mowafy and D. Mohamed, *Sep. Purif. Technol.*, 2014, **128**, 18–24.

40 I. Mayer, *J. Quantum Chem.*, 1986, **29**, 477.

41 X.-W. Chi, Q.-Y. Wu, Q. Hao, J.-H. Lan, C.-Z. Wang, Q. Zhang, Z.-F. Chai and W.-Q. Shi, *Organometallics*, 2018, **37**, 3678–3686.

42 P. W. Huang, C. Z. Wang, Q. Y. Wu, J. H. Lan, G. Song, Z. F. Chai and W. Q. Shi, *Phys. Chem. Chem. Phys.*, 2018, **20**, 1030–1038.